JOURNAL OF SPACECRAFT AND ROCKETS
Vol. 31, No. 1, January–February 1994

Mechanism Synthesis and Two-Dimensional Control Designs of an Active Three-Cable Crane

Li-Farn Yang* and Martin M. Mikulas Jr.†
University of Colorado, Boulder, Colorado 80309

A lunar crane with a three-cable suspension system is investigated to provide a stable end effector for hoisting, positioning, and assembling large components during construction and servicing of a lunar base. The three-cable suspension mechanism consists of a structural framework of three cables pointing to a common point that closely coincides with the suspended payload's center of gravity. The vibrational characteristics of this three-cable device are investigated by comparing a simple two-dimensional suspension model and a swinging pendulum in terms of their analytical natural frequency equations. A study is also made of actively controlling the crane dynamics using two different actuator concepts. Two regulator-type control laws based on Lyapunov control are determined to provide vibration suppression for both dynamic systems. Simulations including initial-valued dynamic responses as well as active control performances are also presented.

Nomenclature

$\tilde{A}$ = system matrix of first-order state equation
B = input matrix of dynamic equations of motion
$\tilde{B}$ = input matrix of first-order state equation
$\tilde{E}$ = inertia matrix of first-order state equation
F = nonlinear forcing matrix of dynamic equations of motion
$\mathfrak{F}$ = natural frequency of a planar three-cable suspension model
$\mathfrak{F}_{\text{pendulum}}$ = natural frequency of single pendulum
G = gain matrix of first-order state equation
g = gravitational constant
h = length of pendulum
I = identity matrix
I = moment of inertia of suspended article
$K(\xi)$ = gravity vector, function of the state vector ξ
$\hat{L}$ = Lagrangian function
$\mathfrak{L}(q,t)$ = Lyapunov function of state vector q and time t
M = inertia matrix of dynamic equations of motion
m = mass of suspended article
m_{si} = masses of sliders 1 and 2 ($i = 1,2$)
O = null matrix
P = positive-definite symmetric weighting matrix of $\mathfrak{L}(q,t)$
Q = semipositive-definite state weighting matrix
q = state vector of first-order state equation,$= [\xi, \dot{\xi}]^T$
R = positive-definite input weighting matrix
T = kinetic energy of mechanical system
V = potential energy of mechanical system
α, β = angular displacements of cables 1 and 2
α_0, β_0 = original angles of α and β
ϵ = displaced angle of cable 1 from α_0, Fig. 5a
ε = distance between center of gravity and the point P, Fig. 5a
θ = angular displacement of structural framework
ξ = state vector of dynamic equations of motion
ρ = gyration radius of suspended article, $= \sqrt{I/m}$
τ = control input vector of dynamic equations of motion
$v_{\text{c.g.}}$ = linear velocity of center of gravity of suspended article
ϕ = angular displacement of H-shaped truss, Fig. 3
$\omega_{\text{c.g.}}$ = angular velocity of suspended article about its center of gravity
$\ell_a, \ell_b, \ell_c, \ell_d, \ell_e$ = lengths of $\overline{AD}$, $\overline{AB}$, $\overline{CD}$, $\overline{BC}$, $\overline{GH}$

Received Jan. 21, 1992; revision received Dec. 7, 1992; accepted for publication Dec. 17, 1992.

*Research Associate, Center for Space Construction.
†Professor, Center for Space Construction. Fellow AIAA.

Introduction

FUTURE lunar base or Mars base missions will likely involve off loading large massive modules from a landing site and moving them to designated areas for construction into an operational base. Because of the remoteness of the bases there will be very little if any direct involvement of astronauts in these operations. Thus the machinery for conducting these operations must be capable of highly stable and/or automated operations. In Ref. 1 a crane concept is presented for automated and precision operations in the zero gravitational field of space, whereas in Ref. 2 a concept is presented for a crane to operate on a planetary surface where gravitational effects must be taken into account. For a zero-g environment an efficient crane takes the form of a long slender beam. In the presence of a gravitational field such as on the surface of a planet there is a large steady static load component for which the crane must be designed. The most efficient structural form for carrying large steady loads is a set of tension members and compression members configured to hold the load with the lowest possible load in each member. In Earth-based construction operations, large

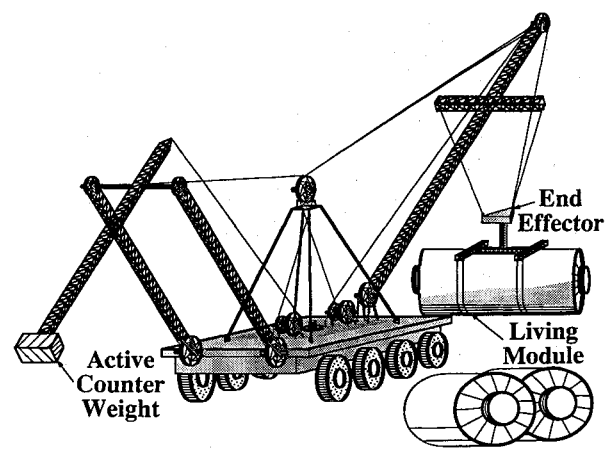

Fig. 1 Counter-balanced actively controlled lunar crane.

cranes with a single vertical support cable are commonly used and the design methodology for such cranes is well documented (see Ref. 3). With such a crane, only a single degree of freedom (the vertical) is positively controlled. The other five payload degrees of freedom are precision positioned by several workers holding onto the payload with guy lines. In Refs. 4–6 a study is conducted of a large crane suitable for automated operations in the heavy construction industry and in the ship building industry. The particular crane concept presented in Ref. 4 has six cables attached to the payload so that all six degrees of freedom can be positively controlled. Although a six-cable crane does provide positive control for all degrees of freedom, it also requires that all six cables be controlled.

In Ref. 2 an alternate crane concept with three cables is presented. For the three-cable crane, three degrees of freedom are positively controlled whereas the other three derive their stiffness from the nonlinear geometric stiffness of the cable crane system.

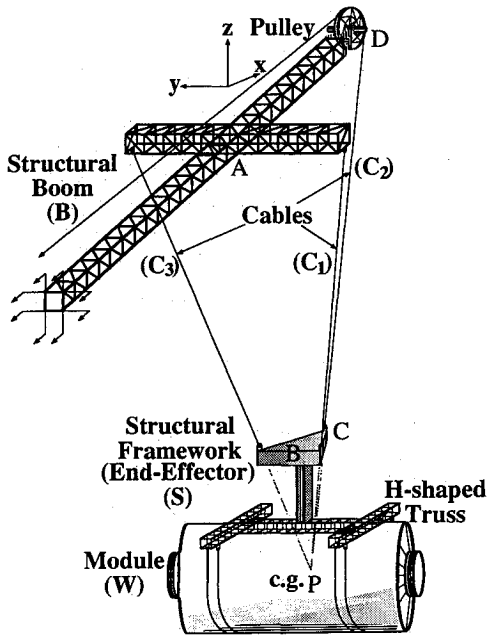

Fig. 2 Three-cable suspension system.

Figure 1 shows the three-cable crane studied in Ref. 2. This crane has an articulated counterweight mechanism on one side, and an end effector suspended by a three-cable mechanism attached to the main boom and to two points on a cross structural boom. The overturning moment of the payload exerted on the lunar crane is counteracted by a counterweight carried at the tip of the articulated mechanism, which will reduce the weight of such a crane. Figure 2 shows a perspective of the three-cable suspension system. The vibrational characteristics and mechanism synthesis as well as control design of this crane system incorporating two different actuator devices form the basis of investigation that is reported in this paper.

The three-cable suspension system undergoes the pendulum-type vibrations as a single pendulum does, if displaced or disturbed from its equilibrium state. For comparison to the single pendulum frequency solution, the three-cable suspension system was simplified into a symmetric two-dimensional model facilitating the derivation of a closed-form solution to natural frequency. This closed-form solution provides insight into the physical parameters which govern the natural frequency; for instance, the elevation, mass, and moment of inertia of the suspended article. Such a simple analysis, conducted for this two-dimensional model, serves as a background for investigating the vibrational characteristics of the three-cable suspension system.

Dagalakis et al.[6] proposed a servo-driven x-y table along with a rotary joint as the vibration compensation device for a robot crane. In the work of Ref. 6, complex actuator-sensory design is included to make the entire electromechanical crane system very cumbersome to deal with; therefore, only experimentally tuned gains can be used in closed loop. Unlike this approach, two different actuator mechanisms as shown in Figs. 3 and 4 are considered in this paper for the active vibrational control design of the three-cable suspension system. The first is an H-shaped truss in conjunction with an extendibly driven longeron; the second is a set of sliders, or linear actuators, on three radial tracks. These actuators drive these two different mechanisms to restore the equilibrium of the crane system under the control command. Their Lagrange's equations of motion are derived for the control designs and dynamic simulations. Lyapunov's theory of asymptotic stability[7,8] is applied to the derivation of control algorithms in designing active controllers for both system dynamics. Initial-valued dynamic responses and control simulations are implemented with an excitation such as an initial angular displacement on the structural framework for comparison. Vibrational suppression of the three-cable suspension system is then accomplished in conjunction with the two different active actuator designs.

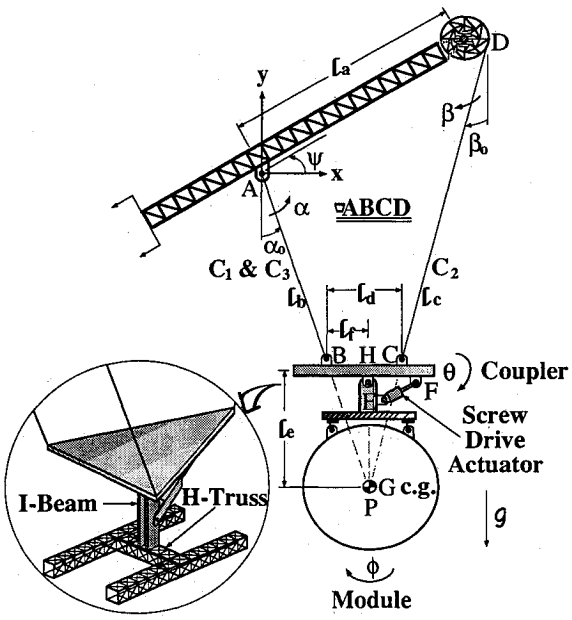

Fig. 3 Active three-cable suspension system with an H-shaped truss.

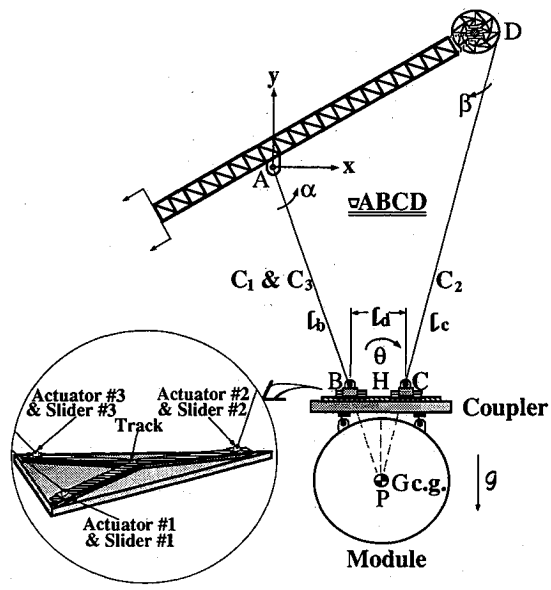

Fig. 4 Active three-cable suspension system with three sliders.

Three-Cable Suspension System Crane Concept

As discussed in Ref. 2, some type of a multiple cable crane will probably be required for planetary base construction and operation. In the present paper, attention is restricted to studying the dynamics and controls of a three-cable suspension system crane. First, an analytical study is made of static equilibrium as well as the dynamic characteristics of this three-cable suspension device without consideration of actuators. Then, actuators are integrated into the three-cable suspension system by means of an H-shaped truss in conjunction with an extendible longeron or three sliders on radial tracks (see Figs. 3 and 4). Dynamics studies of these two different actuator designs are conducted toward the control analysis in generating two stable closed-loop systems.

Figure 2 shows a three-dimensional perspective of a three-cable suspension system in static equilibrium. In Fig. 2, the three-cable suspension device consists of: 1) a structural boom B, 2) a lightweight structural framework acting as an end effector S, 3) three cables C_i, $i=1, 2, 3$, and 4) a suspended article, such as a module W.

The cylindrical module in Fig. 2 is statically equilibrated by a triangular framework S formed from the three connecting cables C_i, $(i=1, 2, 3)$. Cable C_2 wraps around a pulley on the tip of the structural boom B, and cables C_1 and C_3 are connected to two ends of a rectangular truss crossing the structural boom B at the point A. Moreover, cables C_1 and C_3 lie symmetrically with respect to the structural boom B as viewed along the x axis. The three cables provide the upward forces to counterbalance the downward gravitational force on the module. For static equilibrium, the module must be suspended in a way that its center of gravity (c.g.) (point G) is placed along a straight line perpendicularly passing through a common point P at which the extension lines of cables C_1 (or C_3) and C_2 intersect. As a result, the horizontal framework S provides a static end effector to carry the module

The static equilibrium of the module under this three-cable suspension device will not persist in the $x-y$ plane as presented by Fig. 2 if perturbed by any external excitation or disturbance. To study its dynamic characteristics compared to a two-dimensional pendulum problem, the entire three-cable suspension system is constrained in the $x-y$ plane and synthesized as a four-bar-linkage mechanism indicated by $\square ABCD$, which consists of two links $\overline{AB}$ and $\overline{CD}$ as well as a horizontal coupler $\overline{BC}$. The module will rotate about its center of gravity and sway like a pendulum in a direction opposite to the rotation of links $\overline{AB}$ and $\overline{CD}$ within the linkage $\square ABCD$. Unlike the pendulum natural frequency, several parameters in this three-cable suspension system greatly effect the natural frequency, and this will be explored in the next section.

Natural Frequency Analysis of a Planar Model

A closed-form solution to the natural frequency is feasible if the three-cable suspension system in Fig. 2 is simplified into a symmetric planar model as shown in Fig. 5a. The analysis of such a symmetric cable suspension model can serve as a basis as to understanding the vibrational characteristics associated with the three-cable suspension system. In Fig. 5a, a suspended article indicated by its center of gravity is connected to the midspan of the coupler through a rigid link $\overline{HG}$. The coupler is originally kept in the horizontal position using a pair of slant cables. When the equilibrium of the model is perturbed, the article sways around its lowest position while simultaneously rotating about its center of gravity. This is different from a pendulum which only involves swinging in a plane as shown in Fig. 5b. The distinctions of vibration between these two different models in Figs. 5a and 5b will also be apparent by comparing their natural frequency equations.

Natural frequency solution to the model in Fig. 5a is obtained by applying the theory of conservation of energy[9–11] for two critical positions of oscillation indicated by states 1 and 2. State 1 coincides the original static equilibrium configuration ($\square ABCD$), possessing the minimum potential energy in vibration. State 2 displays an extreme configuration ($\square AB'C'D$) with no kinetic energy in vibration, wherein cable 1 is displaced an angle ϵ from $\overline{AB}$ to $\overline{AB'}$, and the coupler is displaced a small angle β from $\overline{BC}$ to $\overline{B'C'}$. In this way, the c.g. of the article is displaced from the point G to G'. Assume that Cartesian coordinates are located at point A without any loss of generality. Then, the total energy at state 2 becomes

$$V_2 = -m\mathcal{G}\,[y_{G'} - y_G] \tag{1}$$

When the article passes through its lowest position relative to state 1, the potential energy as given by Eq. (1) will completely change into the kinetic energy

$$T_1 = {}^1\!/_2\left[m v_{\text{c.g.}}^2 + I\dot{\beta}^2\right] \tag{2}$$

which is composed of the translational and the rotational energies of that swaying article. To equate Eqs. (1) and (2), the potential and kinetic energies as given are described by the angular displacement ϵ and its angular velocity, which have been presented in the Appendix. Note that for a simple harmonic motion the maximum angular velocity $\dot{\epsilon}$ in the kinetic energy at state 1 can be replaced by the product of the maximum angular displacement ϵ and the natural frequency $\mathcal{F}$[9]; i.e., $\dot{\epsilon} = 2\pi\mathcal{F}\epsilon$. Therefore, equating Eqs. (1) and (2) yields the natural frequency equation as

$$\mathcal{F} = \frac{1}{2\pi}\sqrt{\frac{\mathcal{G}\left[\dfrac{\ell_b}{\cos(\alpha_0)} + \tan(\alpha_0)\left(\dfrac{2\ell_b^2\sin^2(\alpha_0)}{\ell_a - 2\ell_b\sin(\alpha_0)}\right) + \ell_e\left(\dfrac{2\ell_b\sin(\alpha_0)}{\ell_a - 2\ell_b\sin(\alpha_0)}\right)^2\right]}{\left[\ell_b\cos(\alpha_0) - \ell_e\left(\dfrac{2\ell_b\sin(\alpha_0)}{\ell_a - 2\ell_b\sin(\alpha_0)}\right)\right]^2 + \rho^2\left[\dfrac{2\ell_b\sin(\alpha_0)}{\ell_a - 2\ell_b\sin(\alpha_0)}\right]^2}} \tag{3}$$

Equation (3) indicates that the magnitude of the natural frequency is a function of the mass and moment of inertia of the suspended article. However, the natural frequency for a pendulum (see Fig. 5b), whose pendulum length is consistent with the same height h as that from $\overline{AD}$ to the common point P in Fig. 5a, is simply governed by

$$\mathcal{F}_{\text{pendulum}} = \frac{1}{2\pi}\sqrt{\frac{\mathcal{G}}{h}} \tag{4}$$

From the geometry of $\square ABCD$, it can be determined that: $\{[2\ell_b\sin(\alpha_0)]/[(\ell_a - 2\ell_b\sin(\alpha_0)]\} = [(\ell_a - \ell_d)/\ell_d]$, $\cos(\alpha_0) = [(h-\ell_c)/\ell_b]$, $\tan(\alpha_0) = (\ell_a/2h)$, and $[(h-\ell_c)/\ell_c] = [(\ell_a - \ell_d)/\ell_d] \Rightarrow \ell_c = (h\ell_d/\ell_a)$. By substituting Eq. (4) into Eq. (3) and changing the geometric variables as just shown, the natural frequency as shown in Eq. (3) can be rewritten without the angular displacement α_0, such as

$$\mathcal{F} = \sqrt{\frac{\left(\dfrac{\ell_b}{h-\ell_h}\right)\left[\ell_h h + \dfrac{\ell_a^2}{4}\right] + \ell_e h}{\varepsilon^2 + \rho^2}}\,\mathcal{F}_{\text{pendulum}}, \quad \ell_h = \ell_e + |\varepsilon|, \text{ if } \varepsilon \geq 0$$
$$= \ell_e + |\varepsilon|, \text{ otherwise} \tag{5}$$

Hence, Eq. (5) indicates that the natural frequency solution to Fig. 5a is a product of the pendulum natural frequency and a modifica-

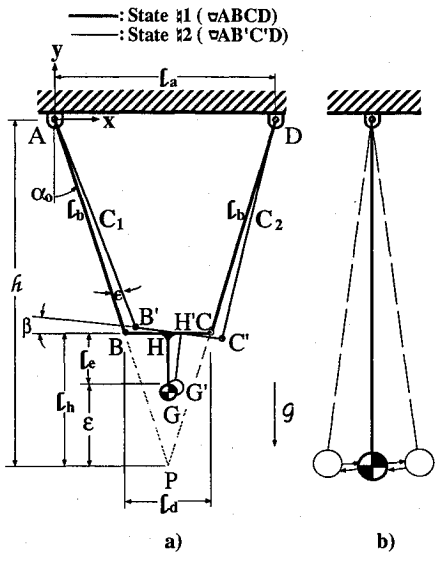

Fig. 5 Symmetric cable suspension system.

tion factor associated with the system geometry. Now, one case is considered: if the geometry of the linkage $\square ABCD$ is known, the natural frequency becomes a function of two variables ℓ_e and ε that can locate the c.g. position. Also, it can be seen that the natural frequency reaches a maximum value as the distance ε becomes zero in the denominator of Eq. (5). This corresponds to the case where the center of gravity of the article and the common point P of the cables coincide, and the resulting maximum natural frequency for $\varepsilon = 0$ can be written as

$$\mathcal{F}_{\max} = \left(\frac{h}{\rho}\right)\frac{1}{\cos\alpha_0\sqrt{(h/\ell_h)-1}}\mathcal{F}_{\text{pendulum}} \tag{6}$$

where ℓ_h can be computed by $^1/_2\cot(\alpha_0)\ell_a$.

Based on Eq. (5), Fig. 6 presents four symmetric "bell-shaped" curves of natural frequencies for four different values of moment of inertia as the distance ε changes from -120 to 120 in. A block inside Fig. 6 summarizes the model parameters of this symmetric cable suspension model. In Fig. 6, for each curve, it can be seen that the highest natural frequency occurs near a value of $\varepsilon = 0$. In addition, the natural frequency decreases with increasing values of the moment of inertia for the same distance ε, which does not exist in the single pendulum problem.

Dynamics of Active Three-Cable Suspension Systems

In this section, the attention is focused at integrating active actuators into a three-cable suspension system. The study considers two different actuator mechanisms and the derivation of their dynamic equations of motion. One mechanism as shown in Fig. 3 is featured by an H-shaped truss in conjunction with a screw-drive actuator underneath the structural framework, and another mechanism as shown in Fig. 4 consists of three sliders with the radial tracks above the structural framework. For both system dynamics, the control laws are taken into account to command the actuators for suppressing the vibrational motions. Control simulations of these two cases will be implemented to verify the feasibilities of these actuators in conjunction with the control designs.

Active Three-Cable Suspension System with an H-Shaped Truss

This subsection deals with the dynamics analysis of an active three-cable suspension system equipped with an H-shaped truss accommodating a screw-drive actuator, such as shown in Fig. 3. The I beam is attached to the structural framework using a pivot at the location H. A screw-drive actuator is set up along an extendible longeron. Two pivots are required to connect the extendible longeron to the structural framework and the I beam at two locations F and E, respectively. Therefore, the screw-drive actuator can extend and contract the extendible longeron to rotate the module about the pivot at the location H. The suspended article, which is shown as a module in Fig. 3, is placed to rest at the common point P underneath an H-shaped truss. Cables 1 and 3, overlapping as viewed from the z axis, can be treated as a single cable for the following derivation of the dynamic equations. The entire suspension system will involve two-degree-of-freedom nonlinear dynamics containing the Coriolis, centrifugal forces, and the kinematic nonlinearity.[8,12]

In Fig. 3, the synthesis of the linkage $\square ABCD$ formed by the structural framework and cables 1 and 2 results in a kinematic relationship to determine the angular velocity of the module. Assume that the angular displacements of the coupler and the H-shaped truss, i.e., θ and ϕ, are selected as two independent variables to describe the motion of the entire system. Furthermore, both bases $\overline{FH}$ and $\overline{EH}$ in ΔFEH have the same length which is equivalent to $\ell_e/2$. The kinematics of the linkage $\square ABCD$ is synthesized by a vectorial equation: $AB+BC+CD+AD=0$, and therein the angular velocities of cables 1 and 2 can be determined in terms of that of the coupler and be expressed as

$$\dot{\beta} = \mathfrak{A}\dot{\theta} \quad \text{and} \quad \dot{\alpha} = \mathfrak{B}\dot{\theta} \tag{7}$$

where

$$\mathfrak{A} = -\left(\frac{\ell_d}{\ell_c}\right)\left[\frac{\cos(\alpha+\theta)}{\sin(\alpha+\beta)}\right] \quad \text{and} \quad \mathfrak{B} = \left(\frac{\ell_d}{\ell_b}\right)\left[\frac{\cos(\theta-\beta)}{\sin(\alpha+\beta)}\right] \tag{8}$$

From Eqs. (7) and (8), the linear velocity of the module at the common point P (or c.g.) can then be written as

$$v_{c.g.} = \sqrt{(\mathcal{C}^2+\mathcal{D}^2)\dot{\theta}^2+\ell_e^2\dot{\phi}^2-2\ell_e[\mathcal{C}\cos(\theta+\phi)+\mathcal{D}\sin(\theta+\phi)]\dot{\theta}\dot{\phi}} \tag{9}$$

where

$$\mathcal{C} = \ell_b\cos(\alpha)\mathfrak{B}-\ell_f\sin(\theta)-\ell_e\cos(\theta+\phi) \tag{10}$$

$$\mathcal{D} = -\ell_b\sin(\alpha)\mathfrak{B}+\ell_f\cos(\theta)-\ell_e\sin(\theta+\phi) \tag{11}$$

The angular velocity of module about its center of gravity can be readily expressed by

$$\omega_{c.g.} = \dot{\theta}+\dot{\phi} \tag{12}$$

Applying Lagrange's equation of motion,[8,11,12] the Lagrangian function for this active three-cable suspension system becomes

$$\hat{L} = T-V \tag{13}$$

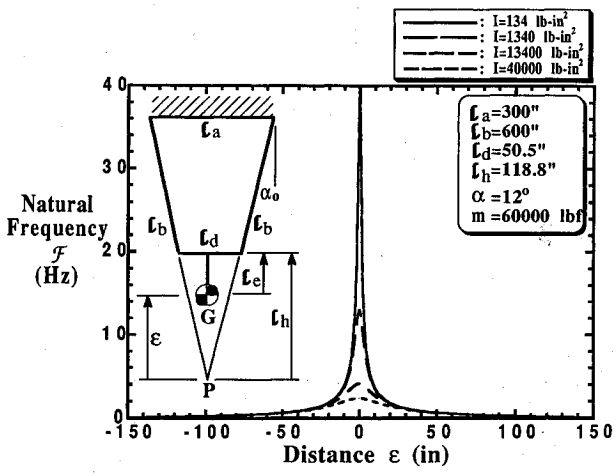

Fig. 6 Natural frequency distribution of a symmetric cable suspension model for the different moments of inertia vs c.g. location.

where the kinetic energy T and the potential energy V are

$$T = {}^1/_2 m v_{c.g.}^2 + {}^1/_2 I \omega_{c.g.}^2 \tag{14}$$

$$V = m\mathcal{G}\{\ell_b[\cos(\alpha) - \cos(\alpha_0)] + \ell_f \sin(\theta) + \ell_e[\cos(\theta+\phi) - 1]\} \tag{15}$$

Both translational and rotational motions contribute to the kinetic energy in Eq. (14) whereas the potential energy in Eq. (15) results from the change of the module elevation. Based on the Lagrangian from Eq. (13), the dynamic equations of motion in matrix form may be written as

$$M\ddot{\xi} + K(\xi) = B\tau + F \tag{16}$$

where ξ denotes a state vector $[\theta, \phi]^T$, and the τ denotes a control input force provided by the screw-drive actuator. The inertia matrix and input, gravity, as well as nonlinear force vectors become

$$M = \begin{bmatrix} m(\mathcal{C}^2 + \mathcal{D}^2) + I - m\ell_e[\mathcal{C}\cos(\theta+\phi) + \mathcal{D}\sin(\theta+\phi)] + I \\ \text{symmetry} \qquad\qquad m\ell_e^2 + I \end{bmatrix} \tag{17}$$

$$B = \begin{bmatrix} -\sin\left(\frac{\pi}{4} - \frac{\theta}{2}\right)\left[\ell_f + \frac{\ell_e}{2}\right] \\ -\frac{\ell_e}{2}\cos\left(\frac{\theta}{2}\right) \end{bmatrix} \tag{18}$$

$$K(\xi) = m\mathcal{G}\begin{bmatrix} \ell_b\mathcal{B}\sin(\alpha) - \ell_f\cos(\theta) + \ell_e\sin(\theta+\phi) \\ \ell_e\sin(\theta+\phi) \end{bmatrix} \tag{19}$$

$$F = m\begin{bmatrix} -2(\mathcal{C}\dot{\mathcal{C}} + \mathcal{D}\dot{\mathcal{D}})\dot{\theta} + \ell_e f\dot{\phi} \\ \ell_e f\dot{\theta} \end{bmatrix} \tag{20}$$

where

$$f = \cos(\theta+\phi)[\dot{\mathcal{C}} + \mathcal{D}(\dot{\theta}+\dot{\phi})] + \sin(\theta+\phi)[\dot{\mathcal{D}} - \mathcal{C}(\dot{\theta}+\dot{\phi})]$$

$$\dot{\mathcal{C}} = \ell_b[\cos(\alpha)\mathcal{B} - \sin(\alpha)\mathcal{B}\dot{\alpha}] - [\ell_f\cos\theta - \ell_e\sin(\theta+\phi)]\dot{\theta} + \ell_e\sin(\theta+\phi)\dot{\phi}$$

$$\dot{\mathcal{D}} = -\ell_b[\sin(\alpha)\mathcal{B} + \cos(\alpha)\mathcal{B}\dot{\alpha}] - [\ell_f\sin(\theta) + \ell_e\cos(\theta+\phi)]\dot{\theta} - \ell_e\cos(\theta+\phi)\dot{\phi}$$

$$\mathcal{B} = -\left(\frac{\ell_d}{\ell_b}\right)\left[\frac{\sin\theta - \beta}{\sin\alpha + \beta}\dot{\theta} + \frac{\cot\alpha + \theta}{\sin\alpha + \beta}\dot{\beta} + \dot{\alpha} + \frac{\cos(\theta-\beta)\cot(\alpha+\beta)}{\sin(\alpha+\beta)}\right]$$

The nonlinearities existing in the inertia matrix M and gravity vector $K(\xi)$ are associated with the kinematic nonlinearity.[8,12] The nonlinear force vector F includes the Coriolis and the centrifugal forces, and the parameters $\dot{\mathcal{C}}$, $\dot{\mathcal{D}}$ and $\dot{\mathcal{B}}$ are the time derivatives of Eqs. (8), (10), and (11).

Active Three-Cable Suspension System with Three Sliders

A slider mechanism such as shown in Fig. 4 may also be applicable for actively damping the three-cable suspension system. In Fig. 4, three actuators drive the three cables, attached to three sliders, along the radial tracks above the structural framework. Sliders 1 and 3 will move simultaneously under a control command, so that cables 1 and 3 always overlay as viewed from the z axis during the control process. Sliders 1 and 3 are regarded as a single slider as shown in Fig. 4 for the derivation of the dynamic equations. The module initially suspended at the common point P is attached to the structural framework. Angles α, β, and θ as defined in the preceding case are selected as the independent variables to describe the entire system dynamics. Hence, this three-cable suspension system equipped with the slider mechanism will possess three degrees of freedom.

The vectorial equation $AB+BC+CD+AD=0$ still holds for synthesizing the kinematics of the linkage $\square ABCD$ except that the distances ℓ_d and ℓ_f are now permitted to vary. Differentiating this equation with respect to time produces the relative velocity ℓ_d between sliders 1 and 2 on the structural framework, which is:

$$\dot{\ell}_d = -\ell_b\cos(\alpha+\theta)\dot{\alpha} - \ell_c\cos(\theta - B)\dot{\beta} \tag{21}$$

The linear velocity of the module can then be written:

$$v_{c.g.} = \sqrt{(\mathfrak{M}\dot{\alpha} + \mathcal{P}\dot{\beta} + \mathcal{R}\dot{\theta})^2 + (\mathfrak{N}\dot{\alpha} + \mathcal{Q}\dot{\beta} + \mathcal{S}\dot{\theta})^2} \tag{22}$$

The parameters accompanied by the angular velocities in Eq. (22) are

$$\mathfrak{M} = \ell_b[\cos(\alpha) - \cos(\theta)\cos(\alpha+\theta)] \tag{23}$$

$$\mathcal{P} = -\ell_c\cos(\theta)\cos(\theta-\beta)$$

$$\mathfrak{N} = -\ell_b[\sin(\alpha) + \sin(\theta)\cos(\alpha+\theta)] \tag{24}$$

$$\mathcal{Q} = -\ell_c\sin(\theta)\cos(\theta-\beta)$$

$$\mathcal{R} = -\ell_d\sin(\theta) - \ell_e\cos(\theta) \tag{25}$$

$$\mathcal{S} = -\ell_d\cos(\theta) - \ell_e\sin(\theta)$$

The angular velocity of the module consistent with that of the structural framework is $\omega_{c.g.} = \dot{\theta}$. The velocity of each slider can be substituted by multiplying the corresponding cable angular velocity together with the cable length, since sliders 1 and 2 are pinned to the tips of cables 1 and 2. For the system as illustrated in Fig. 4, the kinetic energy T and the potential energy V can be expressed by

$$T = {}^1/_2\left(m v_{c.g.}^2 + I\dot{\omega}_{c.g.}^2 + m_{s_1}\ell_b^2\dot{\alpha}^2 + m_{s_2}\ell_c^2\dot{\beta}^2\right) \tag{26}$$

$$V = m\mathcal{G}\{\ell_b[\cos(\alpha) - \cos(\alpha_0)] + \ell_f\sin(\theta) + \ell_e[\cos(\theta) - 1]\} + m_{s_1}\mathcal{G}\ell_b[\cos(\alpha) - \cos(\alpha_0)] + m_{s_2}\mathcal{G}\ell_c[\cos(\beta) - \cos(\beta_0)] \tag{27}$$

where angles α_0 and β_0 are the original angles of cables 1 and 2 under the static equilibrium. Therefore, the Lagrangian for this system, as given by Eq. (13), is obtained so that the dynamic equations of motion, as presented by Eq. (16), can then be derived with the state vector $\xi = [\theta, \alpha, \beta]^T$ and the control input vector $\tau = [\tau_1, \tau_2]^T$, in which two driving forces τ_1 and τ_2 are generated by the actuators on sliders 1 and 2. As a sequence of derivation, the matrices M, B, K, and F are achieved and written as

$$M = \begin{bmatrix} m(\mathcal{R}^2 + \mathcal{S}^2) + I & m(\mathfrak{M}\mathcal{R} + \mathfrak{N}\mathcal{S}) & m(\mathcal{P}\mathcal{R} + \mathcal{Q}\mathcal{S}) \\ & m(\mathfrak{M}^2 + \mathfrak{N}^2) + m_{s_1}\ell_b^2 & m(\mathfrak{M}\mathcal{P} + \mathfrak{N}\mathcal{Q}) \\ \text{symmetry} & & m(\mathcal{P}^2 + \mathcal{Q}^2) + m_{s_2}\ell_c^2 \end{bmatrix} \tag{28}$$

$$K(\xi) = \begin{bmatrix} m\mathcal{G}[\ell_b \mathcal{B}\sin(\alpha) - \ell_f \cos(\theta) + \ell_e \sin(\theta)] \\ m_{s_1}\mathcal{G}\ell_b \sin(\alpha) \\ m_{s_2}\mathcal{G}\ell_c \sin(\beta) \end{bmatrix} \tag{29}$$

$$F = m\dot{\xi}\begin{bmatrix} 2(\mathcal{P}\dot{\mathcal{P}} + \mathcal{S}\dot{\mathcal{S}}) & \mathcal{R}\dot{\mathfrak{M}} + \mathfrak{M}\dot{\mathcal{R}} + \mathcal{S}\dot{\mathfrak{N}} + \mathfrak{N}\dot{\mathcal{S}} & \mathcal{R}\dot{\mathcal{P}} + \mathcal{P}\dot{\mathcal{R}} + \mathcal{S}\dot{\mathcal{Q}} + \mathcal{Q}\dot{\mathcal{S}} \\ & 2(\mathfrak{M}\dot{\mathfrak{M}} + \mathfrak{N}\dot{\mathfrak{N}}) & \mathcal{P}\dot{\mathfrak{M}} + \mathfrak{M}\dot{\mathcal{P}} + \mathcal{Q}\dot{\mathfrak{N}} + \mathfrak{N}\dot{\mathcal{Q}} \\ \text{symmetry} & & 2(\mathcal{P}\dot{\mathcal{P}} + \mathcal{Q}\dot{\mathcal{Q}}) \end{bmatrix} \tag{30}$$

$$B = \begin{bmatrix} 0 & 0 \\ -\ell_b \cos(\theta + \alpha) & 0 \\ 0 & -\ell_c \cos(\theta - \beta) \end{bmatrix} \tag{31}$$

where

$$\dot{\mathfrak{M}} = \ell_b - \left[\sin(\alpha) - \cos(\theta)_{s_1}\right]\dot{\alpha} + \left[\sin(\theta)\, c_1 + \cos(\theta)_{s_1}\right]\dot{\theta}$$

$$\dot{\mathfrak{N}} = -\ell_b\left[\cos(\alpha) - \sin(\theta)_{c_1}\right]\dot{\alpha} + \left[\cos(\theta)\, c_1 - \sin(\theta)_{s_1}\right]\dot{\theta}$$

$$\dot{\mathcal{P}} = -\ell_c - [\sin(\theta)\, c_2 + \cos(\theta)\, s_2]\,\dot{\theta} + \cos(\theta)\, s_2\dot{\beta}$$

$$\dot{\mathcal{Q}} = -\ell_c\,[\cos(\theta)\, c_2 - \sin(\theta)\, s_2]\,\dot{\theta} - \sin(\theta)\, c_2\dot{\beta}$$

$$\dot{\mathcal{R}} = -\sin(\theta)\,\ell_d - [\ell_d \cos(\theta) - \ell_e \sin(\theta)]\,\dot{\theta}$$

$$\dot{\mathcal{S}} = \cos(\theta)\,\ell_d - [\ell_d \sin(\theta) + \ell_e \cos(\theta)]\,\dot{\theta}$$

$$s_1 = \sin(\alpha + \theta), \qquad c_1 = \cos(\alpha + \theta)$$

$$s_2 = \sin(\theta - \beta), \qquad c_2 = \cos(\theta - \beta)$$

In Eq. (30), the time-derivative parameters, i.e., $\dot{\mathfrak{M}}, \dot{\mathfrak{N}}, \dot{\mathcal{P}}, \ldots, \dot{\mathcal{S}}$ are derived from Eqs. (23–25) through the differentiation process. Based on the dynamic equations from Eq. (16), the initial-valued dynamic response can then be simulated by imposing the initial angular displacement or initial impact on the system.

The determination of the proper feedback control law must be taken into account to link the relationship between the control input vector and the state vector toward accomplishing the closed-loop dynamic equations for those two different dynamic systems as developed in this section. To provide active damping for a disturbed system, Lyapunov-based control algorithms such as those used in Ref. 8 are introduced next.

Active Vibrational Control Design

Two active three-cable suspension systems as presented in the preceding section require active control designs enabling their actuators to suppress vibrations resulting from external disturbances. A control technique based on the theory of Lyapunov's "second method"[7] will provide the stability criteria to determine the control laws for the actuators in those two dynamic systems. Such a Lyapunov-based controller acts as a regulator in performing an asymptotically stable closed-loop system, in which the perturbed system is capable of returning to its equilibrium state under the control process. Linear control design will be utilized because of its simplicity and feasibility in hardware implementation. Hence, the nonlinear dynamic equations in Eq. (16) will be linearized to be compatible with the linear control algorithms.

For small vibrational motion, the nonlinearities residing in the dynamic equations can be neglected or approximated by their linear counterparts for the control analysis of both active three-cable suspension systems. Assume that the inertia matrix M and the input matrix B in Eq. (16) are properly linearized and their linearized counterparts are denoted by $\bar{M}$ and $\bar{B}$ respectively, whereas the gravity vector $K(\xi)$ is approximated into $\bar{K}\xi$ and $F \approx 0$. Now these linear dynamic equations thus linearized from Eq. (16) will be rearranged into the first-order state equations[8] that are consistent with the following control algorithms. They are

$$\tilde{E}\dot{q} = \tilde{A}q + \tilde{B}\tau, \qquad \tau = Gq \tag{32}$$

where

$$\tilde{E} = \begin{bmatrix} I & O \\ O & \bar{M} \end{bmatrix}, \qquad \tilde{A} = \begin{bmatrix} O & I \\ -\bar{K} & O \end{bmatrix}, \qquad \tilde{B} = \begin{bmatrix} O \\ \bar{B} \end{bmatrix} \tag{33}$$

Note that the cumbersome inversion of the inertia matrix can be avoided in conducting the control analysis[8,13] for the dynamic system as given by Eq. (32) because the linearized inertia matrix $\bar{M}$ has been included in a symmetric and positive-definite matrix $\tilde{E}$ instead of in the system matrix $\tilde{A}$. The control input vector τ in Eq. (32) will then be fed back into the nonlinear dynamic equations when the control gain matrix G is determined following the next Lyapunov-based control analysis.

In general, the control approach based on Lyapunov's asymptotic stability theory[7] begins with specifying an energy function $\mathcal{L}(q,t)$ (or Lyapunov function) which must satisfy: 1) $\mathcal{L}(q,t) > 0$ for $q \neq q_e$, 2) $\mathcal{L}(q_e,\infty) = 0$, and 3) $\dot{\mathcal{L}}(q_e, t) \leq 0$ for $q \neq q_e$, where q_e represents the state vector of equilibrium. Hence, the objective

of defining the Lyapunov function is to seek an active control input to perform a dissipative closed-loop system in the asymptotic stability. A quadratic Lyapunov function[8] may be defined as

$$\mathcal{L}(q,t) = q^T\left[\tilde{E}^T P \tilde{E}\right] q \tag{34}$$

where the weighting matrix P plays a key role to tune the control gain matrix G in the following procedure. According to the third stability criterion, differentiating Eq. (34) with respect to time and substituting Eq. (32) into the resulting time-derivative equation yields

$$\dot{\mathcal{L}}(q,t) = q^T\left[\tilde{A}^T P \tilde{E} + \tilde{E}^T P \tilde{A}\right] q + \tau^T \tilde{B}^T P \tilde{E} q + q^T \tilde{E}^T P \tilde{B} \tau \tag{35}$$

The last two terms on the right-hand side in Eq. (35) can be combined into the first bracketed term in a quadratic form of the state vector q by assigning the control input vector τ as

$$\tau = Gq \qquad \text{and} \qquad G = -R^{-1}\tilde{B}^T P \tilde{E} \tag{36}$$

where the weighting matrix R is capable of tuning the magnitude of control effort. Substitution of Eq. (36) into Eq. (35) provides

$$\dot{\mathcal{L}}(q,t) = q^T\left[\tilde{A}^T P \tilde{E} + \tilde{E}^T P \tilde{A} - 2\tilde{E} P \tilde{B} R^{-1} \tilde{B}^T P^T \tilde{E}^T\right] q$$

$$= -q^T Q q \le 0 \tag{37}$$

The matrix inside the bracket in Eq. (37) is the well-known algebraic Riccati equation that can result in a negative matrix Q to tune the decreasing rate of Lyapunov function, which can adjust the rate of system vibrational suppression. In Eq. (37), the inequality holds for the given control gain matrix G as given in Eq. (36). The matrix P is solved in the Riccati equation by specifying the matrices Q and R. Substituting the weighting matrices P and R into Eq. (36) generates a control gain matrix G in Eq. (32) that results in an active control input for those nonlinear dynamic systems developed in the preceding section. As a result, the conditions of Lyapunov's asymptotic stability are all satisfied. In other words, the Lyapunov-based control input vector in Eq. (36) provides the system with asymptotic stability, which will bring the perturbed system from any arbitrarily initial state to the desired static equilibrium state.

Simulation Results

Two different active actuator designs have been incorporated into the three-cable suspension system to damp the dynamic motion during the crane operation, and their dynamic equations of motion have been derived. For both system dynamics, Lyapunov-based control laws have been determined to guarantee their system stabilities in the Lyapunov's sense. Two kinds of simulations subjected to an initial angular displacement imposed on the structural framework were implemented with and without control for comparison.

To implement the control simulations for those two active three-cable suspension systems, the same model parameters are specified to be: $\ell_a = 300$ in., $\ell_b = 510$ in., $\ell_c = 680$ in., $\ell_d = 50$ in., $\ell_e = 141.38$ in., $\ell_f = 44.35$ in., $m = 60{,}000$ lbf, $m_{s_i} = 10$ lbf ($i = 1, 2$), $I = 805{,}803$ lbm-in.^{2}, $\psi = 40$ deg, and $\alpha_0 = 17.42$ deg.

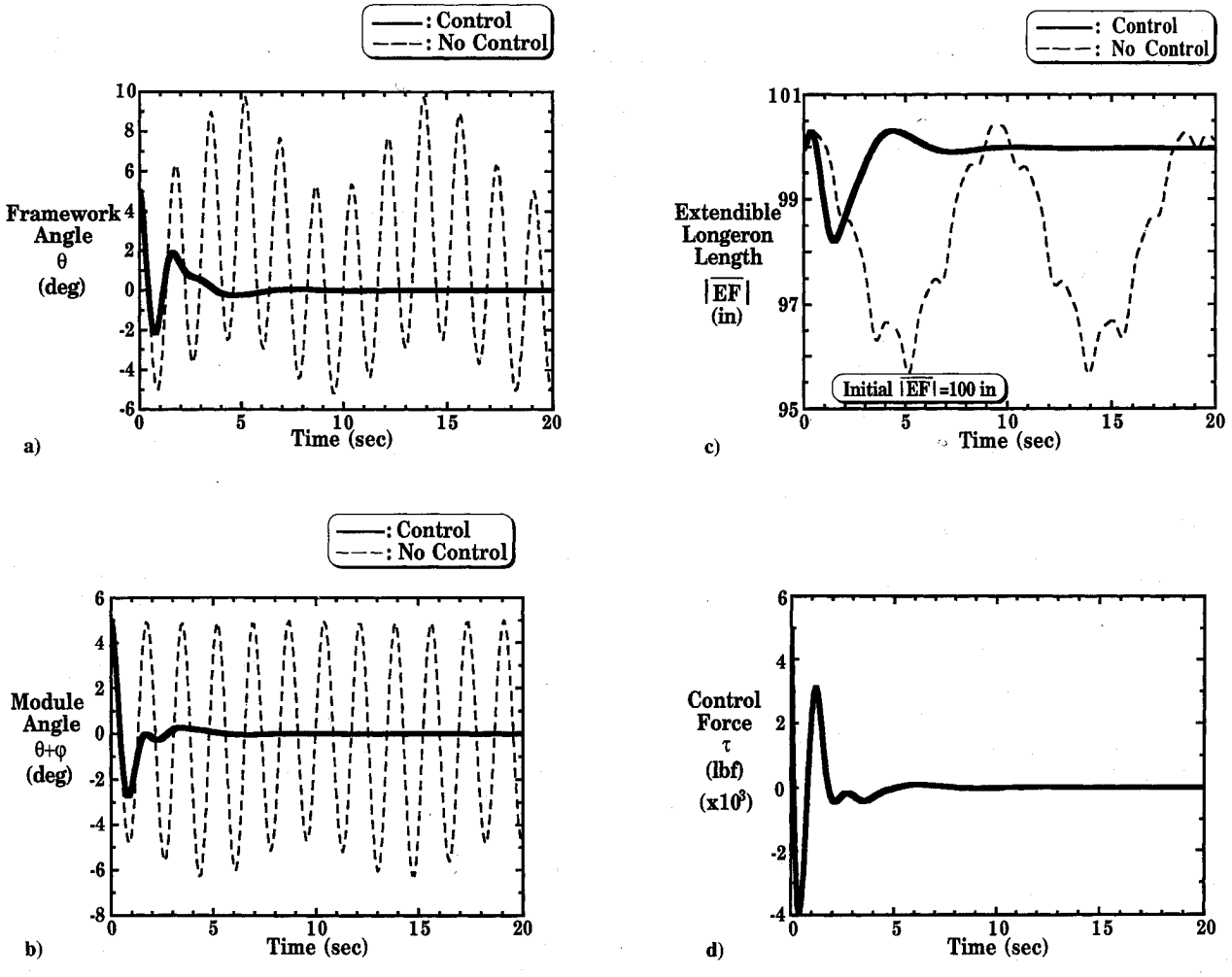

Fig. 7 Control simulation results of an active three-cable suspension system with an H-shaped truss.

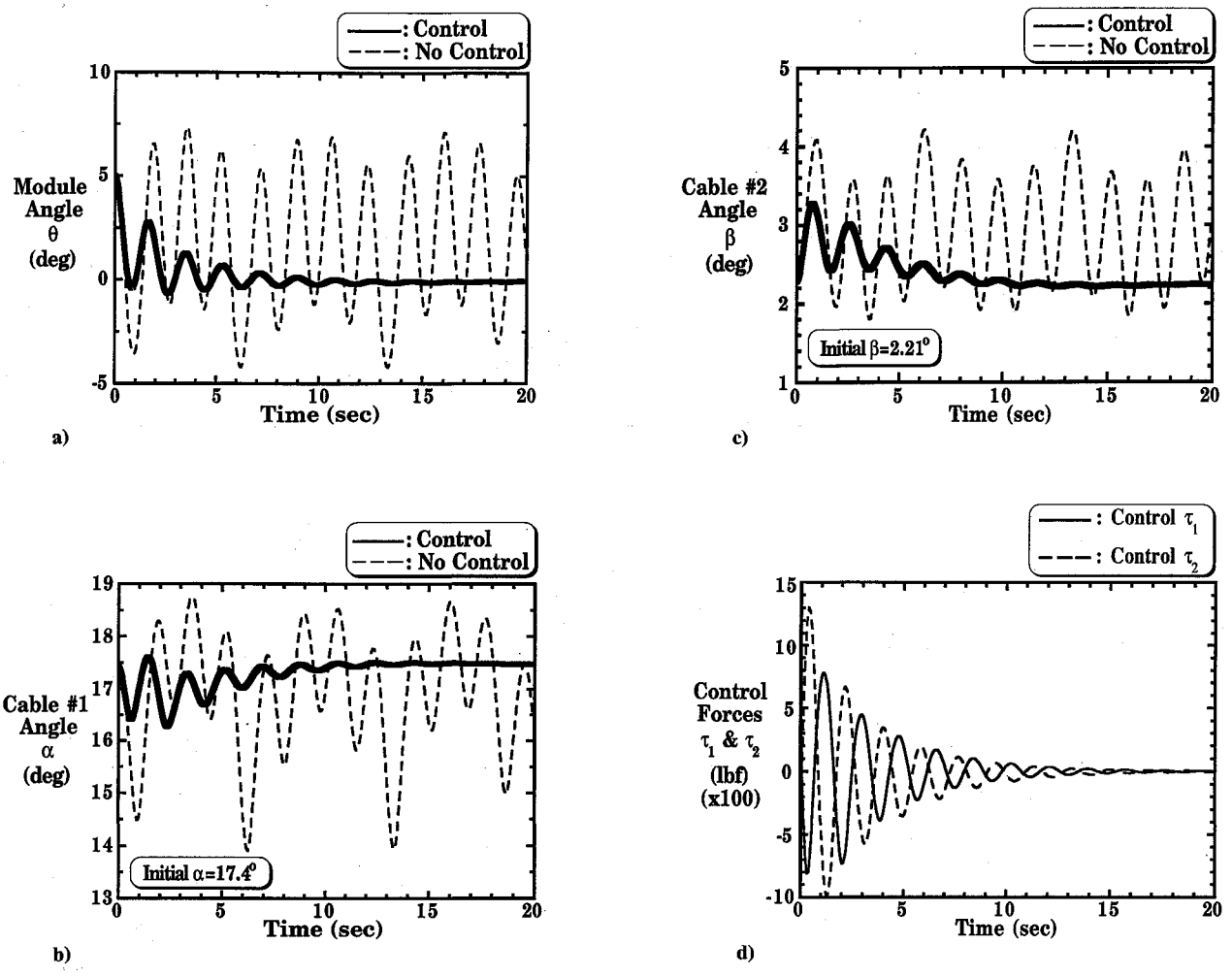

Fig. 8 Control simulation results of an active three-cable suspension system with three sliders on radial tracks.

Active Three-Cable Suspension System with an H-Shaped Truss

The weighting matrices relative to Lyapunov-based control law for an active three-cable suspension system incorporating a screw-drive actuator on an H-shaped truss are summarized as follows

$$R = 1$$

$$Q = \text{diag}\,[10^6, 10^5, 1, 3]\,10^4 \tag{38}$$

$$P = 10^{10}\begin{bmatrix} 0.4813 & 0.5234 & 0.0187 & -0.0742 \\ & 1.9070 & 0.0228 & 0.0354 \\ \text{symmetry} & & 0.0942 & 0.2733 \\ & & & 0.9890 \end{bmatrix}$$

where the matrix P is determined by solving the Riccati equation with given state and input weighting matrices Q and R. Then, substitution of those matrices into Eq. (36) leads to the determination of the Lyapunov-based control law such as

$$G = [58{,}158,\ 17{,}680,\ 19{,}338,\ -26{,}600] \tag{39}$$

The simulation is carried out by specifying an initial angular displacement of 5 deg to the angle of the structural framework. Figures 7a–7d are the simulation results of this active three-cable suspension system. The results associated with the use of Lyapunov-based control are indicated by the solid lines, whereas those without the presence of control are denoted by the dotted lines. Figure 7a shows the angular displacement of the structural framework. The trajectory without the presence of control demonstrates an oscillatory motion which is composed of two vibrational modes at two different frequencies: 0.12 and 0.56 Hz. However, such an oscillatory motion is suppressed within 5 s when an active controller is enacted. For the behavior in Fig. 7a, the controller creates two small overshoots in the first 2 s and suppresses the residual vibration in the rest of the simulation. Moreover, the maximum magnitude in the first overshoot is reduced by 50% under the control process. The time history of angular displacement of the module is shown in Fig. 7b. The module oscillates about its center of gravity within the range from −7 to 5 deg when the controller is turned off. However, the module returns to its original position after an oscillation with 50% reduction in 5 s during the control process. Therefore, it can be seen that, in the control process, the extendible longeron extends and contracts not only to guide the structural framework back into its horizontal position but also to suppress the vibrational motion of the module. Figures 7c and 7d show the longeron stroke and control force, respectively. The original length of the longeron is 100 in. The longeron stroke with no control oscillates with the structural framework and module. It can be observed that the longeron driven by the screw-drive actuator rapidly extends a small stroke at first, then contracts a large stroke from 0.5 to 3 s, and extends once more until 7 s. The control force exerted on the longeron starts at 6000 lbf and ends up with 0 lbf after 8 s. As a result, a successful control simulation in suppressing the dynamic motion of the three-cable suspension system is easily accomplished using a screw-drive actuator.

Figures 7a–7d indicate that a screw-drive actuator design in conjunction with an H-shaped truss is capable of suppressing the dynamic motion of the initially perturbed three-cable suspension system. Simulation results of the three-cable suspension system equipped with three actuators on three sliders will be presented next.

Active Three-Cable Suspension System with Three Sliders

In this simulation setup, three identical sliders carrying three active actuators move along radial tracks on the structural framework for implementing system dynamic suppression when the system equilibrium is perturbed. Two sliders aligned in the z direction move simultaneously under a control command. The weighting matrices together with the resulting Lyapunov-based control gain matrix for the slider actuators are listed as follows:

$$R = \text{diag}\,[1, 1]$$

$$Q = \text{diag}\,[1, 1, 1, 1, 1, 1]\,10^{8}$$

$$P = 10^{9}\begin{bmatrix} 0.4249 & 0.0052 & 0.0148 & -0.0488 & 0.0494 & -0.1705 \\ & 0.1653 & -0.0056 & -0.0415 & 0.0868 & -0.0207 \\ & & 0.4835 & 0.2420 & -0.0159 & 1.1190 \\ & \text{symmetry} & & 0.3272 & -0.0787 & 1.1837 \\ & & & & 0.1435 & -0.0848 \\ & & & & & 5.4524 \end{bmatrix} \tag{40}$$

$$G = \begin{bmatrix} -7180 & -9897 & 1354 & -318 & -16{,}456 & 7105 \\ 2113 & -1354 & -9898 & -1542 & -1679 & -47{,}829 \end{bmatrix}$$

The initial-valued dynamic responses without the presence of control have been simulated under the same excitation as that in the preceding subsection and are compared with those using the feedback control. The simulation results are given in Figs. 8a–8d. Figure 8a is the angular displacement of the module. It can be observed that the module oscillates six times and its motion is suppressed to rest at its original position after 9 s under the control process. The dynamic time history as shown in Fig. 8a demonstrates the capability of the slider actuators in suppressing vibrational motion of the module. Figure 8b shows the angular displacement of cable 1 and Fig. 8c those of cable 2. Since two cables move together with the sliders, it can be seen from Figs. 8b and 8c that sliders 1 and 2 under the control process move alternatively within a range of 9 in. and stop in 13 s. Two cables (or sliders) move toward or away from each other rather than oscillating in phase. However, the oscillatory motion between two sliders cannot be damped out without the use of control. Moreover, slider 1 seems to be more active than slider 2 because the module is initially located closer to slider 2 than slider 1. As the controllers are enacted, the driving forces start acting on sliders 1 (3) and 2 and their results are shown in Fig. 8d. It can be seen that both maximum magnitudes of the control forces in Fig. 8d are one-third of that for the single actuator as shown in Fig. 7d, but the control time for restoring the equilibrium of this three-cable suspension system may be longer.

The vibrational behaviors appearing in the time-history responses of module, cables, and sliders from Figs. 8a–8c have been considerably suppressed through the Lyapunov-based control design. The results in Figs. 8a–8d thus validate the applicability of the slider mechanism for restoring the equilibrium of the three-cable suspension system.

Conclusions

In this paper a lunar crane concept with three suspension cables is presented and analyzed. This three-cable crane has three degrees of freedom positively constrained by the cables whereas the remaining three degrees of freedom derive their stiffness from the nonlinear stiffness of the cable crane system. To provide a basic insight into the behavior of such a crane, a two-dimensional version of the crane with only two cables was analyzed. An exact solution was obtained for the lowest natural frequency of the system, and results are presented in parametric form to demonstrate vibrational characteristics of the multiple cable suspension system. A study was conducted on the active vibration suppression of the degrees of freedom which are not positively constrained by the suspension cables. Two different actuator concepts were studied utilizing Lyapunov-based control algorithms, and a comparison of the two is made. General conclusions which were drawn from the study are as follows:

1) The magnitude of the natural frequency of a mass suspended by three cables is a strong function of geometry of the attachment points as well as the magnitude of the mass and the magnitude of the mass moment of inertia. This is in contrast to a simple pendulum where the magnitude of the natural frequency is only a function of the pendulum length.

2) The magnitude of the natural frequency of a mass suspended by three cables increases significantly as the position of the center of gravity nears the intersection point of the three cables.

3) Because of the large number of parameters that affect the system dynamics, there are a wide variety of control schemes that can be implemented into the crane to accomplish active vibration suppression. In the present paper two sample control schemes were studied.

4) Results from the two control simulations indicate that suppressing the dynamic motion of the three-cable crane is a rather straightforward process, however, other control schemes need to be studied. Also, work to date has not included structural flexibilities of the crane and this could significantly complicate the control process.

Appendix: Energies T_1 and V_2 in the Natural Frequency Analysis

Assume that cable 1 is displaced on a small angle ϵ from its original angle α_0 as displayed in Fig. 5a. In the displaced linkage $\square AB'C'D$, the displaced angle of the coupler between $\overline{BC}$ and $\overline{B'C'}$ can be written by

$$\tan(\beta) = \frac{2\ell_b \sin(\alpha_0)}{\ell_b - 2\ell_b \sin(\alpha_0)} \sin(\epsilon)$$

$$\Rightarrow \beta = \frac{2\ell_b \sin(\alpha_0)}{\ell_a - 2\ell_b \sin(\alpha_0)} \epsilon \tag{A1}$$

for the small angles β and ϵ. The angular velocity $\dot{\beta}$ can be replaced by $\dot{\epsilon}$ through Eq. (A1). Hence, the linear velocity of the suspended article resulting from its two $x - y$ components at a certain instant can be written by

$$v_{c.g.} = \left[\ell_b \cos(\alpha_0) - \ell_e\left(\frac{2\ell_b \sin(\alpha_0)}{\ell_a - 2\ell_b \sin(\alpha_0)}\right)\right]\dot{\epsilon} \tag{A2}$$

By using Eqs. (A1) and (A2), the kinetic energy T_1 at state 1 and the potential energy V_2 at state 2 as given by Eqs. (1) and (2) are then expressed by

$$T_1 = {}^1/_2 m \left\{ \left[\ell_b \cos(\alpha_0) - \ell_e \left(\frac{2\ell_b \sin(\alpha_0)}{\ell_a - 2\ell_b \sin(\alpha_0)} \right) \right]^2 + I \left[\frac{2\ell_b \sin(\alpha_0)}{\ell_a - 2\ell_b \sin(\alpha_0)} \right]^2 \right\} \dot{\epsilon}^2 \tag{A3}$$

$$V_2 = {}^1/_2 m \mathcal{G} \left[\frac{\ell_b}{\cos(\alpha_0)} + \frac{2\ell_b^2 \sin^2(\alpha_0) \tan(\alpha_0)}{\ell_a - 2\ell_b \sin(\alpha_0)} + \ell_e \left(\frac{2\ell_b \sin(\alpha_0)}{\ell_a - 2\ell_b \sin(\alpha_0)} \right)^2 \right] \epsilon^2 \tag{A4}$$

Acknowledgments

The authors wish to acknowledge the support of this investigation through NASA Grant NAGW-1388 from NASA Headquarters and through a donation from the Shimizu Corporation. The authors thank Charbel Farhat for his assistance in the symbolic derivation of the frequency equation of the pendulum motion.

References

[1]Mikulas, M. M., Jr., Davis, R. C., and Greene, W. H., "A Space Crane Concept: Preliminary Design and Static Analysis," NASA TM-101498, Nov. 1988.

[2]Mikulas, M. M., Jr., and Yang, L.-F., "Conceptual Design of a Multiple Cable Crane for Planetary Surface Operations," NASA TM-104041, Jan. 1991.

[3]Shapiro, H. I., Shapiro, J. P., and Shapiro, L. K., *Cranes & Derricks*, 2nd ed., McGraw-Hill, New York, 1991.

[4]Unger, J., Dagalakis, N. G., Tsai, T.-M., and Lee, J. D., "Optimum Stiffness Study for a Parallel Link Robot Crane under Horizontal Force," *Proceedings of the Second International Symposium on Robotics and Manufacturing: Research, Education, and Applications* (Albuquerque, NM), Nov., 1988, pp. 1037–1046.

[5]Dagalakis, N. G., Albus, J. S., Wang, B.-L., Unger, J., and Lee, J. D., "Stiffness Study of a Parallel Link Robot Crane for Shipbuilding Applications," *Proceedings of the Seventh International Conference on Offshore Mechanics and Arctic Engineering* (Houston, TX), Feb. 1988, pp. 29–37.

[6]Dagalakis, N. G., Albus, J. S., Goodwin, K. R., Lee, J. D., Tsai, T.-M., Abrishamian, H., Bostelman, R., and Yancey, C., "Robot Crane Technology (Final Report)," National Institute of Standards and Technology, NIST Tech. Note 1267, U.S. Dept. of Commerce, Washington, DC, July 1989.

[7]Kalman, R. E., and Bertram, J. E., "Control System Analysis and Design via the 'Second Method' of Lyapunov," *Journal of Basic Engineering*, Vol. 82, No. 2, June 1960, pp. 371–393.

[8]Juang, J.-N., Yang, L.-F., and Huang, J.-K., "Lyapunov-Based Control Designs for Flexible-Link Manipulators," AIAA Paper 89-1214, April 1989.

[9]Beer, F. P., and Johnston, E. R., Jr., *Vector Mechanics for Engineers*, 3rd ed., McGraw-Hill, New York, 1977.

[10]Meirovitch, L., *Analytical Methods in Vibrations*, 3rd ed., MacMillan, New York, 1971.

[11]Greenwood, D. T., *Principles of Dynamics*, Prentice-Hall, Englewood Cliffs, NJ.

[12]Huang, J.-K., Yang, L.-F., and Juang, J.-N., "Large Planar Maneuvers for Articulated Flexible Manipulators," AIAA Paper 88-4119, Aug. 1988.

[13]Oshman, Y., Inman, D. J., and Laub, A. J., "Square Root State Estimation for Second-Order Large Space Structures Models," *Journal of Guidance, Control, and Dynamics*, Vol. 12, No. 5, 1989, pp. 698–708.